This is a peer-reviewed, accepted author manuscript of the following article: Ma, H. H., Weng, S. M., Li, P., Li, X. F., Wang, Y. X., Yew, S. H., Chen, M., McKenna, P., & Sheng, Z. M. (2020). Growth, saturation, and collapse of laser-driven plasma density gratings. Physics of Plasmas, 27(7), [73105]. https://doi.org/10.1063/5.0004529

Growth, saturation and breaking down of laser-driven plasma density gratings

H. H. Ma[1,2], S. M. Weng[1,2],* P. Li[3], X. F. Li[1,2], Y. X. Wang[1,2], S. H. Yew[1,2], M. Chen[1,2], P. McKenna[4], and Z. M. Sheng[1,2,4,5]†

[1] *Key Laboratory for Laser Plasmas (MoE), School of Physics and Astronomy, Shanghai Jiao Tong University, Shanghai 200240, China*

[2] *Collaborative Innovation Center of IFSA, Shanghai Jiao Tong University, Shanghai 200240, China*

[3] *Research Center of Laser Fusion of China Academy of Engineering Physics, Mianyang, SiChuan, 621900, China*

[4] *SUPA, Department of Physics, University of Strathclyde, Glasgow G4 0NG, UK and*

[5] *Tsung-Dao Lee Institute, Shanghai 200240, China*

(Dated: August 22, 2019)

Two nonlinear theoretical models are presented to describe the time evolution of a plasma density grating induced by intersecting high power laser beams. The first model is based on the fluid equations, while the second is a kinetic model that adopts the particle mesh method. It is found that both models can describe the plasma density grating formation at different stages, well beyond the linear growth stage. However, the saturation of the plasma density grating, which is attributed to the kinetic effect of "ion wave-breaking", can only be predicted by the second model based on the particle mesh method. Using the second model, we also find that the saturation time of the plasma density grating increases with the plasma density and decreases with the laser intensity. The results from these two nonlinear theoretical models are compared and verified using particle-in-cell simulations.

I. INTRODUCTION

Since the invention of chirped pulse amplification technology [1], laser peak power and focused intensity have increased many orders of magnitude in the last three decades. Nowadays, many laser systems in the world can deliver petawatt (PW) laser pulses [2], which can be tightly focused to ultrahigh intensities $\sim 10^{21}$ W/cm^2. The interactions of such intense laser pulses with materials bring about rich physical phenomena and many prospective applications [3, 4]. However, the manipulation of such laser pulses becomes more and more challenging for conventional solid-state optical components which are susceptible to optical damage at high laser intensities. For silica, which is most widely used material in solid-state optics, laser-induced damage threshold of energy fluence is on the level of 10 J/cm^2 in the femtosecond to picosecond regime. In order to keep the laser energy fluence below this damage threshold, the diameters of solid-state optical components are usually required to be meter-scale for multi-PW laser systems. In contrast, plasmas resulted from the ionization of materials can sustain much higher laser intensities than solid crystals. Consequently, plasma-based optical components for the manipulation of ultra-high-power laser pulses can be made more compact than their conventional solid-state optical components. As a result, plasma-based optics are attracting growing attention [5–22].

To date, a lot of novel schemes based on plasma optics have been proposed for the manipulation or amplification of intense laser pulses. Plasma mirrors are widely used for enhancing the temporal-intensity contrast of intense laser pulses [5, 6], Raman or Brillouin scattering in laser-plasma interactions are studied for the amplification of laser pulses [7–10], cross-beam energy transfer in plasmas is studied for tuning the implosion symmetry of inertial confinement fusion targets [11, 12], and magnetized plasmas are proposed for the polarization control of ultra-high-power laser pulses [13, 14] or the amplification of intense laser pulses [15]. In particular, two intersecting intense laser pulses in plasma can induce a plasma density modulation and form a periodic density structure, i.e., plasma density grating (PDG) [16]. Such a PDG can sustain a relatively high laser intensity exist in a quasi-steady state for several picoseconds. Therefore, it becomes an attractive approach for the manipulation of femtosecond intense laser pulses, and is studied for broad applications such as the plasma compressor, the plasma polarizer and waveplate, and the transient plasma photonic crystals for high-power laser [17–22].

Although many novel potential applications based on the PDG are proposed, the physics of its formation and evolution is still not fully investigated. So far, the analytical models based on the linearization approximation of fluid equations are widely adopted in the studies of the PDG formation [16, 23, 24]. These linear analytical models are competent for describing the PDG formation process in the initial linear stage. However, the evolution of the PDG can be highly nonlinear when the plasma density peaks are many times larger than the initial plasma density in the later stage. Further, kinetic effects such as ion wave breaking can develop, which are responsible for the final collapse of the PDG. Until now, little attention has been paid to the PDG development at the nonlinear stage, and still less to the stage after the ion wave breaking. In this study, we develop two nonlinear theoretical models for describing the PDG evolution beyond the linear stage. The first model is obtained by com-

* wengsuming@gmail.com
† z.sheng@strath.ac.uk

bining the assumption of the quasi-neutrality of plasmas and the two-fluid plasma model. Without the linearization approximation, the growth process of the PDG with sharp density peaks much larger than the initial plasma density is described well by this fluid-based model. To include kinetic effects, the particle-mesh (PM) method is adopted in the second model [25]. The wave equation is solved for the electromagnetic field, while the equations of motion are solved for the electrons and ions as done in the particle-in-cell (PIC) simulations. Since the particles are treated individually, the saturation and the wave breaking of the PDG can be reproduced by the second model. This study extends the understanding of the whole process of the PDG evolution including its growth, saturation and collapse, which could be of great benefit to the design and analysis of related experiments.

To analyze the evolution of the PDG, we organize the manuscript as follows: two theoretical models based on the fluid equations and the particle-mesh method are constructed in Sec. II. These two models are verified by particle-in-cell simulations in Sec. III, with an emphasis on the saturation and collapse of the PDG in the later stage. The dependence of the PDG saturation time on the laser intensity and the plasma density is clarified. Finally, some discussion and a short summary is presented in Sec. IV.

II. NONLINEAR MODELS OF THE PLASMA DENSITY GRATING EVOLUTION

In principle, PDGs could be induced by intersecting laser beams in plasmas in a variety of scenarios. For simplicity, in this work the PDG is assumed to be induced by two oppositely propagating laser beams through a homogeneous plasma. One beam is propagating in the positive x-axis and one in the negative x-axis. The laser beams are assumed to have the vector potentials $\boldsymbol{A_1} = A_1\cos(\omega_1 t - k_1 x)\boldsymbol{e}_y$ and $\boldsymbol{A_2} = A_2\cos(\omega_2 t + k_2 x)\boldsymbol{e}_y$, with the same frequency and wave number, i.e., $\omega_1 = \omega_2 = \omega$ and $k_1 = k_2 = k$. Here A_1 and A_2 are the electric field amplitudes of laser beams 1 and 2, respectively. The wave number in plasma is determined by $k = k_0\sqrt{1 - n_0/n_c}$, where k_0 is the wave number in vacuum, n_0 is the background plasma density and $n_c = \omega^2\varepsilon_0 m_e/e^2$ is the critical plasma density corresponding to the laser frequency ω. Here m_e is the electron mass and ε_0 is the permittivity of free space. The superposition of these two laser beams can form a standing wave, which will induce a ponderomotive force on the electrons. Introducing the normalized vector potential $a_{1,2} = eA_{1,2}/m_e c^2$, this ponderomotive force can be written as [16]

$$\boldsymbol{F}_p = m_e c^2 a_1 a_2 k \sin(2kx)\boldsymbol{e}_x. \tag{1}$$

The normalized vector potential a is related to the laser intensity I as $a \simeq (I\lambda^2/1.37\times 10^{18}[\mathrm{W}\mu\mathrm{m}^2/\mathrm{cm}^2])^{1/2}$, where λ is the laser wavelength in a vacuum. The above equation indicates that the ponderomotive force induced by two counter-propagating laser beams has a spatial period of π/k, which will result in a spatially periodic modulation of the plasma density, i.e. the PDG formation.

A. Model based on the fluid equations

We first consider the fluid model for the formation of the PDG due to the periodic ponderomotive force. In a cold plasma, the momentum equations for electrons and ions are

$$n_e m_e \frac{\partial v_e}{\partial t} = n_e e\frac{\partial \varphi}{\partial x} - n_e F_p, \tag{2}$$

$$n_i m_i \frac{\partial v_i}{\partial t} = -n_i Z_i e\frac{\partial \varphi}{\partial x}, \tag{3}$$

where φ is the scalar potential of the space-charge field, Z_i is the ion charge number, v_i and v_e are the fluid velocities of ions and electrons, respectively. Since the directions of velocities and forces are all along the x-axis, we ignore the vector symbols of those vectors in Eqs. (2)-(3) and the following derivations.

Assuming the plasma remains quasi-neutral (i.e. $n_e \equiv Z_i n_i$) in the whole process of the PDG development, the sum of the momentum equations for electrons and ions yields

$$m_i \frac{\partial v_i}{\partial t} = -Z_i m_e c^2 a_1 a_2 k \sin(2kx), \tag{4}$$

where the term of electron inertia is omitted since $m_e \ll m_i$. Normalizing the time, frequency, distance, wave number and velocity to $2\pi/\omega$, ω, λ, $2\pi/\lambda$ and c, respectively, the above equation can be rewritten as

$$\frac{\partial v_i}{\partial t} = b\sin(hx) \tag{5}$$

where $b = -2\pi a_1 a_2 k Z_i m_e/m_i$ and $h = 4\pi\sqrt{1 - n_e/n_c}$. The time integration of the above equation gives the fluid velocity for ions $v_i = b\sin(hx)t$. Substituting this into the continuity equation for ions, one can obtain the following initial-value problem

$$\frac{\partial n}{\partial t} + [b\sin(hx)t]\frac{\partial n}{\partial x} = -bh\cos(hx)tn, \tag{6}$$

$$n(x, 0) = n_0, \tag{7}$$

where n is the ion density normalized to n_c, and n_0 is the initial ion density of the homogeneous plasma. Equation (6) is a first order quasi-linear partial differential equation, and it can be rewritten as follows

$$\frac{dt}{d\tau} = 1, \tag{8}$$

$$\frac{dx}{d\tau} = b\sin(hx)t, \tag{9}$$

$$\frac{dn}{d\tau} = -bh\cos(hx)tn, \tag{10}$$

where τ is an intermediate variable, and the initial condition at $\tau = 0$ are $t = 0$, $x = \xi$, and $n = n_0$, respectively.

By the integration of the above equations, the variables of t, x and n can be expressed as the implicit functions of τ and ξ as

$$\tau = t \tag{11}$$

$$\ln\left|\frac{[\tan(hx)-\sin(hx)]\tan(h\xi)\sin(h\xi)}{\tan(hx)\sin(hx)[\tan(h\xi)-\sin(h\xi)]}\right| = \frac{bh}{2}\tau^2, \tag{12}$$

$$n_0 \exp\left\{\int_0^\tau [-bh\cos[hx(\zeta,\xi)]\zeta]d\zeta\right\} = n, \tag{13}$$

For any given time-space coordinates (t, x), the corresponding intermediate variables τ and ξ can be gotten from the first two equations. Substituting these two intermediate variables into Eq. (13), the density of ions n can be obtained finally. That is to say, the plasma density profile at any time can be predicted by Eqs. (11)-(13) during the buildup process of the PDG.

B. Model based on the particle-mesh method

In the above model the plasma is treated as a fluid, therefore, kinetic effects are excluded. In order to embrace kinetic effects and reproduce the saturation and ion wave-breaking of the PDG, another model is developed using the particle-mesh (PM) method. In this particle-mesh model, the plasma is represented by a large number of macro-particles. Then the evolution of the PDG can be resolved by tracking the motion of all macro-particles. Under the assumption of a quasi-neutral plasma, one only has to track the motions of ions as follows

$$\frac{dv}{dt} = \frac{1}{m_i}\boldsymbol{F}_p(x), \tag{14}$$

$$x = \int_0^t v(t')dt' + x_0 \tag{15}$$

where $\boldsymbol{F}_p$ is the ponderomotive force of two counter-propagating laser pulses that given by Eq. (1), and v, x and x_0 are the velocities, coordinates and initial coordinates of each individual ions, respectively. Using the same normalized units used in the first model, the above equations can be rewritten as

$$\frac{dv}{dt} = -b\sin(hx), \tag{16}$$

$$x = \int_0^t v(t')dt' + x_0. \tag{17}$$

The instantaneous velocities and coordinates of each ion can be updated by numerically solving the above integro-differential equations. The plasma density is defined on the discrete meshes, and its value can be obtained by the interpolation of macro-particles to each mesh as done in the PIC simulation.

It is worth pointing out that the incident laser beams will be obviously reflected as the PDG grows. Therefore, the space- and time-dependent laser vector potentials a_1 and a_2 are required for the accurate calculation of the ponderomotive force. For simplicity, we assume a quasi-static steady state for the plasma during the PDG formation. Then during laser propagating in the plasma, their electric fields satisfy the following wave equation [21]

$$\frac{\partial^2 a}{\partial x^2} + 4\pi^2[1-n(x,t)]a = 0, \tag{18}$$

where $a = eE/m\omega c$ is the normalized transverse electric field of the laser beam. As a typical density profile of the PDG, $n(x,t)$ in the above equation is spatially periodic. So the Bloch wave ansatz can be applied to solve Eq. (18), in which the density profile is firstly expanded in Fourier series as follows [21]

$$n(x) = \sum \eta_p e^{i(\frac{2\pi p}{l})x}, p = 0, \pm1, \pm2, \pm3\ldots, \tag{19}$$

where p denotes the p-th Fourier mode, η_p is the p-th order Fourier coefficient, $l = 1/2k$ is the spatial period of the PDG. In our calculation, we truncate at $p = 4$ order for the sake of simplicity. The Fourier coefficients can be calculated numerically for a given density $n(x)$. When a laser beam propagates in a plasma with a spatially periodic structure, its electric field is a Bloch wave, which can be rewritten as

$$a(x) = \sum c_p e^{i(k+\frac{2\pi p}{l})x}, p = 0, \pm1, \pm2, \pm3\ldots, \tag{20}$$

where c_p is the p-th Fourier coefficient, and k is the laser wave number. Substituting Eqs. (19) and (20) into the Eq. (18), a set of algebraic equations can be obtained

$$c_p[-(k+\frac{2\pi p}{a})^2 + 4\pi^2] - 4\pi^2\sum_{p'=-p}^{p} c_{p'}\eta_{p-p'} = 0, \tag{21}$$

for $p = 0, \pm1, \pm2, \pm3, \pm4$. To get a nonzero solution for c_p, the determinant of the above equation should be zero. Consequently, the wave number k is obtained for a set of Fourier coefficients η_p. If the imaginary part of k is not zero, the laser beam will attenuate with the propagation distance x as follows

$$a(x) = e^{-Im(k)x}a_0, \tag{22}$$

where a_0 is the normalized laser vector potential before the attenuation. Combining Eqs. (16)-(22), the plasma density and laser intensity profiles can be updated step by step. Consequently, the evolution of the PDG can be well predicted.

III. VERIFICATION WITH NUMERICAL SIMULATION

To verify the proposed models, the evolution processes of the PDGs predicted by our theoretical models are compared with that obtained from PIC simulations. One-dimensional PIC simulation is conducted using the code Osiris [26]. In the simulation, a simulation box with a

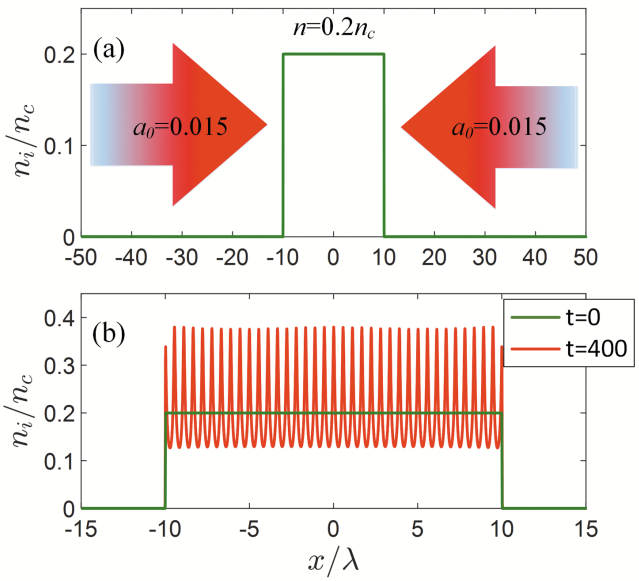

FIG. 1. (a) Laser and plasma parameters used in the PIC simulation. The initial plasma is cold and has a uniform density $n_0 = 0.2n_c$ in $|x| \leq 10\lambda$. Two linearly polarized laser pulses with the same frequency ω and amplitude $a_0 = 0.015$ are launched from two boundaries, as shown by the arrows. (b) The ion density profile obtained from the PIC simulation at $t = 400T_0$ is compared with that at $t = 0$, where $T_0 = 2\pi/\omega$ is the laser wave period.

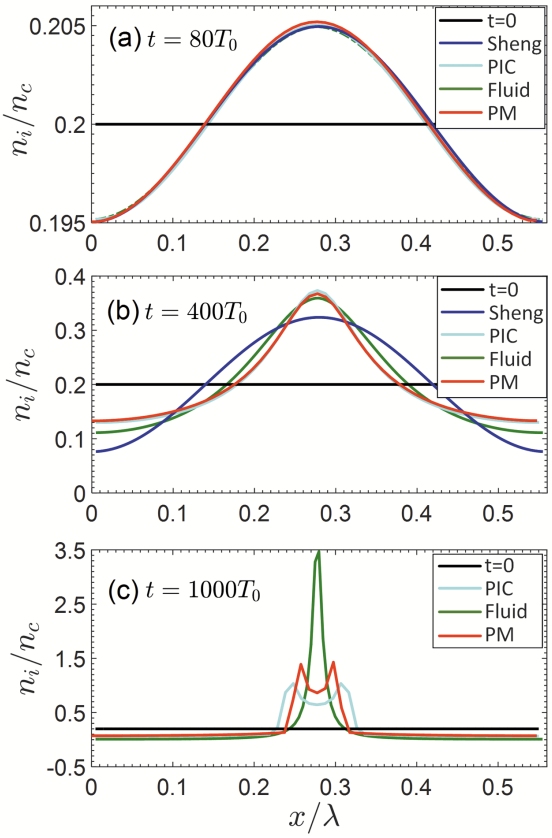

FIG. 2. The ion density profiles of a single cycle of the PDG at the center region $0 < x < \pi/k$ of the simulation box in (a) the early linear growth stage at $t = 80T_0$, (b) the nonlinear growth stage at $t = 400T_0$, and (c) the stage after the wave-breaking at $t = 1000T_0$, respectively. The comparison is made among the results from the PIC simulation (light blue lines), our fluid-based model (green lines), and our kinetic model based on the PM method (red lines). The black lines indicate the ion density profile at $t = 0$, and the results according to the linearized fluid model Eq. (23) (blue lines) are also drawn for comparison in (a) and (b).

dimension of 100λ is located at $x \in [-50\lambda, 50\lambda]$, and a homogeneous plasma is located at the central region of $-10\lambda < x < 10\lambda$. As shown in Fig. 1(a), two linear polarized laser pulses with the same frequency ω and same amplitude a_0 are launched from the left and right boundaries of the simulation box. For convenient comparison with the theoretical models, the laser pulses in the simulation have flat-top profiles and they are long enough so that the PDG has the time to develop, saturate and collapse. The initial plasma is assumed to be cold and the ions are protons. As shown in Fig. 1(b), the ion density profile at $t = 400T_0$ obtained from the PIC simulation confirms the formation of the PDG. The peak density of the PDG at this moment is about twice the uniform density at $t = 0$.

To compare the different models in detail, we zoom in a single cycle of the PDG at the center region $0 < x < \pi/k$ of the simulation box, where $\pi/k = \lambda/2\sqrt{1 - n/n_c} \simeq 0.56\lambda$. In Fig. 2, the ion density profiles at this zoom region obtained from our nonlinear models are compared with that from the PIC simulation. For comparison, we also display the ion density profile predicted by the previous linear fluid model. According to the linearized fluid model [16], the density modulation δn is given by

$$\delta n = \frac{k^2c^2}{\omega_p^2}\frac{m_e}{m_i}a_1a_2\cos(2kx)[4\sin^2(\frac{\omega_p t}{2}) - \omega_p^2t^2]. \quad (23)$$

The above equation defines a density modulation that is always a cosine function of the x-coordinate. This linearized fluid model is applicable for the early stage of the PDG evolution when the density modulation is much smaller than the initial density as shown in Fig. 2(a). If the density modulation is comparable to the initial density as show in Fig. 2(b), however, this linearized fluid model is no longer able to describe the PDG evolution accurately. In contrast, the ion density profiles predicted by our nonlinear models based on the fluid equations and the particle-mesh method are still in good agreement with the results of the PIC simulation.

More importantly, the PIC simulation shows that the peaks of the PDG will split with the increasing of the peak density as shown in Fig. 2(c). This highlights that the PDG will saturate, and its periodic structure will be finally destroyed due to ion wave-breaking. However,

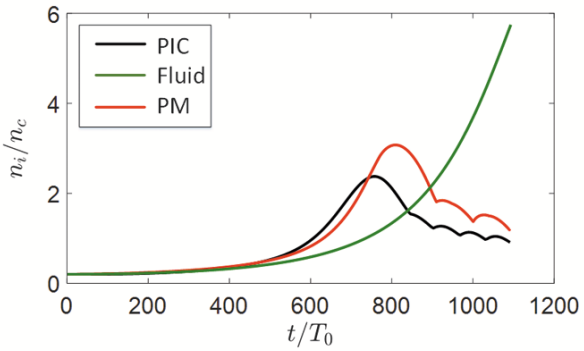

FIG. 3. Time evolution of the peak density of the PDG at the center of the simulation box. The comparison is made among the results from the PIC simulation (black line), our fluid-based model (green line), and our kinetic model based on the PM method (red lines).

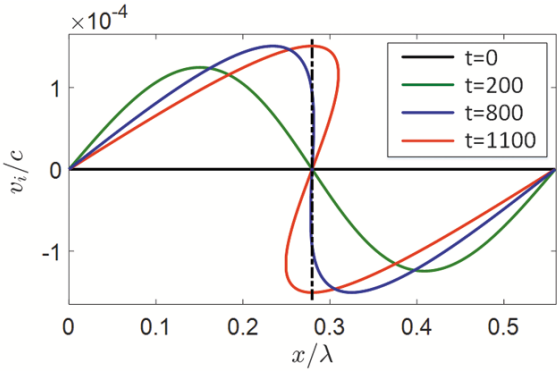

FIG. 4. The ion distributions in the $x - v_x$ phase space obtained from our PM-based kinetic model at some typical times: $t = 0$ as the initial state, $t = 200T_0$ in the growth stage, $t = 800T_0$ around the saturation time when ion wave-breaking occurs, and $t = 1100T_0$ after the wave-breaking.

Fig. 2(c) shows that the PDG peak density calculated by the nonlinear fluid-based model would increase continuously. The cause of this difference is that the wave breaking is a kinetic effect, so it cannot be captured by the fluid-based model. As expected, the wave breaking could be treated by our second model based on the PM method. As a result, the splits of the PDG density peaks is reproduced by the our kinetic model based on the PM method as shown in Fig. 2(c). We also notice that the PDG obtained from the PIC simulation has wider but lower density peaks than the PDG from the PM-based model. This might be because the plasma heating, which tends to dissipate the PDG, is self-consistently included in the PIC simulation.

The time evolution of the peak density of the PDG obtained from different models are compared in Fig. 3. At the early linear stage ($t < 500T_0$), it is found that the peak density of the PDG increases slowly with time, and all models are consistent with each other. At the later stage ($t > 500T_0$), however, the peak density of the PDG obtained from the fluid model seems to increase without limit since the wave breaking effect is not included in this model. In contrast, both the PIC simulation and the PM method are in the category of kinetic model. Therefore, the peak densities of the PDGs obtained from them will reach a maximum after a fast growth (at around $700T_0 < t < 800T_0$) and then begin to decrease. We call this phenomenon the saturation of the PDG, and the time when the PDG peak density reaches its maximum is defined as the saturation time.

Although the peak density of the PDG obtained from the PIC simulation is a little lower than that from our kinetic model based on the PM method due to the plasma heating, we find that the PDG from the PIC simulation develops a little faster than that from our kinetic model based on the PM method. The PDGs from the PIC simulation and the PM method saturate at $t \simeq 740T_0$ and $t \simeq 800T_0$, respectively. This might be because our PM-based kinetic model only handles the attenuation of the laser intensity and doesn't consider the trapping of the laser pulses by the PDG. While the trapping of the laser pulses by the PDG is self-consistently treated by the PIC simulation, which could result in the local enhancement of the laser pulses in the PDG and hence speeds up the development of the PDG.

To better understand the saturation of the PDG, the ion distributions in the $x - v_x$ phase space obtained from our PM-based kinetic model at some different times are displayed in Fig. 4. Under the periodic ponderomotive force of two oppositely propagating laser beams, the ions in the left half region are accelerated while those in the right half region are decelerated as shown in Fig. 4.

Therefore, the density at the center increases and the PDG develops. With the increasing of the peak density, the slope of the ion phase-space distribution at the density peak goes to negative infinity and then reverses its sign at around $t \simeq 800T_0$, where ion trajectories begin to cross each other. This corresponds to the saturation time of the PDG when the maximum of the peak density is achieved as show in Fig. 3. Due to the inertia effect, the ions from the left and right half parts will continue to move across each other. As a result, the ion fluid velocity at a given position, such as the position of the density peak, becomes no longer unique after $t \simeq 800T_0$. In other words, the wave breaking takes place and saturates the PDG.

To study the dependence of the growth rate of the PDG on the plasma density and the laser intensity, we calculate the saturation time of the PDG by our PM-based kinetic model under different plasma densities and laser intensities. The results are displayed in Fig. 5. Except for the laser intensities and plasma densities, other laser-plasma parameters are the same as those used in Figs. 1-4. From Fig. 5, it can be found that the saturation time T_s of the PDG decreases gradually with an increasing laser intensity a_0 for a given plasma density

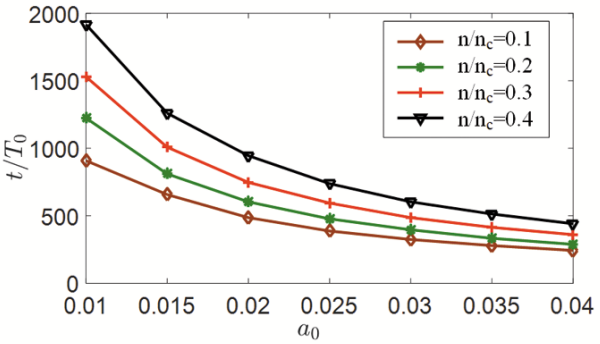

FIG. 5. The saturation time of the PDG with different laser intensity and plasma densities obtained from our PM-based kinetic model. Except for the laser intensities and plasma densities, other laser-plasma parameters are the same as those used in Figs. 1-4.

n_0. While the saturation time T_s of the PDG increases with an increasing plasma density n_0 for a given laser intensity. This is because the saturation will be achieved faster with a stronger ponderomotive force, and Eq. (1) indicates that the ponderomotive force increases with increase in the laser intensity a and the wave number k in plasma, while k decreases with increase in the plasma density n_0. It is worth pointing out that the saturation time of the PDG also depends on other parameters such as the plasma temperature, the ion mass m_i and so on. Using a large number of calculations based on our PM-based kinetic model, the saturation time T_s of the PDG for a cold plasma can be roughly fitted by

$$T_s = \left(0.73 + \frac{M}{3.7}\right)(21.09n + 6.97)a^{-0.16n-0.98}, \quad (24)$$

where $M = m_i/m_p$ is the ion mass normalized to the mass of the proton, and a and n are the normalized laser intensity and initial plasma density, respectively. The above equation can be conveniently used to evaluate the saturation time of the PDG in experiments.

IV. DISCUSSION AND CONCLUSION

A basic assumption adopted in both our fluid-based model and PM-based kinetic model is that the plasma remains quasi-neutral for the entire process of the PDG formation. To verify that this assumption is reasonable, the density difference between the electrons and ions is monitored in the PIC simulation. Defining the maximal relative density difference as

$$\Delta n_{\max} = \max_{|x|\le 10}\left|\frac{n_e - n_i}{n_i}\right|, \quad (25)$$

the time evolution of this difference obtained from the PIC simulation is show in Fig. 6. It is confirmed that the

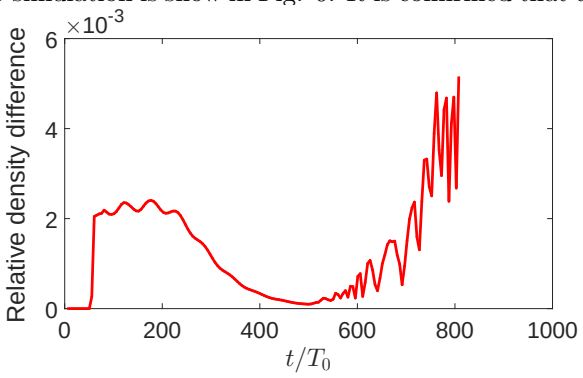

FIG. 6. The time evolution of the maximal relative density difference between the electrons and ions obtained from the PIC simulation.

maximal relative density difference between the electrons and ions is always less than 1% for the entire process of the PDG formation.

In summary, the time evolution of the PDG induced by intersecting laser beams is studied by two newly-constructed nonlinear theoretical models. In the first model, a set of first order quasi-linear partial differential equations is derived from the fluid equations, which can be used to predict the time evolution of the PDG beyond the linear growth stage. In the second model, the PM method is adopted to handle the kinetic effects such as ion wave-breaking. Considering the wave-breaking effect, it is found that the peak density of the PDG will decrease after it reaches a maximum value. That is to say, the saturation of the PDG will take place due to the kinetic effects, and this saturation does not appear in the fluid-based models. Since the wave breaking is well treated using this PM-based kinetic model, it can describe the time evolution of the PDG beyond the saturation time. Further, the dependence of the saturation time of the PDG on the laser intensities a_0 and plasma densities n_0 is investigated using this PM-based kinetic model. It is found that the saturation time of the PDG increases with the plasma density and decreases with the laser intensity. Our study indicates that it is possible to produce the PDG with a life time on the order of picoseconds, which can be used to manipulate intense laser pulses from picoseconds down to femtoseconds.

ACKNOWLEDGMENTS

The work was supported by the National Natural Science Foundation of China (Grant Nos. 11975154, 11675108, 11655002, 11721091, 11535001, and 11775144), Presidential Foundation of the Chinese Academy of Engineering Physics (No. YZJJLX2016008), Science Challenge Project (No.TZ2018005) and EPSRC (Grant No. EP/R006202/1). Simulations have been carried out on the Pi supercomputer at Shanghai Jiao Tong University.

[1] D. Strickland and G. Mourou, Opt. Commun. **55**, 447 (1985).

[2] C Danson, D Hillier, N Hopps, D Neely. High Power Laser Science and Engineering. **3**, e3 (2015).

[3] G. A. Mourou, T. Tajima, and S. V. Bulanov, Rev. Mod. Phys. **78**, 309 (2006).

[4] P. Gibbon, *Short Pulse Laser Interactions with Matter*, (Imperial College Press, 2005).

[5] G. Doumy, F. Quéré, O. Gobert, M. Perdrix, Ph. Martin, P. Audebert, J. C. Gauthier, J.-P. Geindre, and T. Wittmann, Phys. Rev. E. **69**, 026402 (2004).

[6] C. Thaury, F. Quéré, J. -P. Geindre, A. Levy, T. Ceccotti, P. Monot, M. Bougeard, F. Réau, P. d'Oliveira, P. Audebert, R. Marjoribanks and Ph. Martin, Nat. Phys. **3**, 424 (2007).

[7] V. M. Malkin, G. Shvets, and N. J. Fisch. Phys. Rev. Lett. **82**, 4448 (1999).

[8] R. M. G. M. Trines, F. Fiúza, R. Bingham, R. A. Fonseca, L. O. Silva, R. A. Cairns and P. A. Norreys, Nat. Phys. **7**, 87 (2011).

[9] S. Weber, C. Riconda, L Lancia, JR Marques, G. A. Mourou, and J. Fuchs. Phys. Rev. Lett. **111**, 055004 (2013).

[10] G. Lehmann and K. H. Spatschek, Phys. Plasmas **20**, 073112 (2013).

[11] P. Michel, L. Divol, E. A. Williams, S. Weber, C. A. Thomas, D. A. Callahan, S. W. Haan, J. D. Salmonson, S. Dixit, D. E. Hinkel, M. J. Edwards, B. J. MacGowan, J. D. Lindl, S. H. Glenzer, and L. J. Suter. Phys. Rev. Lett. **102**, 025004 (2009).

[12] D. J. Y. Marion, A. Debayle, P.-E. Masson-Laborde1, P. Loiseau1 and M. Casanova1. Phys. Plasmas. **23**, 052705 (2016).

[13] S. M. Weng, Q. Zhao, Z. M. Sheng, W. Yu, S. X. Luan, M. Chen, L. L. Yu, M. Murakami, W. B. Mori, and J. Zhang, Optica **4**, 1086 (2017).

[14] X. L. Zheng, S. M. Weng, Z. Zhang, H. H. Ma, M. Chen, P. McKenna, and Z. M. Sheng, Opt. Express **27**, 19319 (2019).

[15] M. R. Edwards, Y. Shi, J. M. Mikhailova, and N. J. Fisch, Phys. Rev. Lett. **123**, 025001 (2019)

[16] Z. M. Sheng, J. Zhang, D.Umstadt. Appl. Phys. B. **77**, 673 (2003).

[17] H. C. Wu, Z. M. Sheng, and J. Zhang, Appl. Phys. Lett. **87**, 201502 (2005).

[18] H. C. Wu, Z. M. Sheng, Q. J. Zhang, Y. Cang and J. Zhang, Phys. Plasmas **12**, 113103 (2005).

[19] P. Michel, L. Divol, D. Turnbull, and J. D. Moody, Phys. Rev. Lett. **113**, 205001 (2014).

[20] D. Turnbull, P. Michel, T. Chapman, E. Tubman, B. B. Pollock, C. Y. Chen, C. Goyon, J. S. Ross, L. Divol, N. Woolsey, and J. D. Moody, Phys. Rev. Lett. **116**, 205001 (2016).

[21] G. Lehmann and K. H. Spatschek. Phys. Rev. Lett. **116**, 225002 (2016).

[22] G. Lehmann and K. H. Spatschek. Phys. Rev. E. **97**, 063201 (2018).

[23] P. Michel, W. Rozmus, E. A. Williams *et al.*, Phys. Plasmas **20**, 056308 (2013).

[24] G. Lehmann and K. H. Spatschek. Phys. Plasmas **26**, 013106 (2019).

[25] R. W. Hockney, J. W. Eastwood, *Computer Simulation Using Particles*, (CRC Press, 1985).

[26] R. A. Fonseca, L. O. Silva and F. S. Tsung *et al.*, Lect. Not. Comput. Sci. **2331**, 342 (2002).